Trapping and Release of CO_2 Guest Molecules by Amorphous Ice

S. Malyk, G. Kumi, H. Reisler,* and C. Wittig*

Department of Chemistry, University of Southern California, Los Angeles, California 90089

Received: May 26, 2007; In Final Form: September 20, 2007

Interactions of $^{13}CO_2$ guest molecules with vapor-deposited porous H_2O ices have been examined using temperature-programmed desorption (TPD) and Fourier transform infrared (FTIR) techniques. Specifically, the trapping and release of $^{13}CO_2$ by amorphous solid water (ASW) has been studied. The use of $^{13}CO_2$ eliminates problems with background CO_2. Samples were prepared by (i) depositing $^{13}CO_2$ on top of ASW, (ii) depositing $^{13}CO_2$ underneath ASW, and (iii) codepositing $^{13}CO_2$ and H_2O during ASW formation. Some of the deposited $^{13}CO_2$ becomes trapped when the ice film is annealed. The amount of $^{13}CO_2$ trapped in the film depends on the deposition method. The release of trapped molecules occurs in two stages. The majority of the trapped $^{13}CO_2$ escapes during the ASW-to-cubic ice phase transition at 165 K, and the rest desorbs together with the cubic ice film at 185 K. We speculate that the presence of $^{13}CO_2$ at temperatures up to 185 K is due to $^{13}CO_2$ that is trapped in cavities within the ASW film. These cavities are similar to ones that trap the $^{13}CO_2$ that is released during crystallization. The difference is that $^{13}CO_2$ that remains at temperatures up to 185 K does not have access to escape pathways to the surface during crystallization.

1. Introduction

Interactions of molecules with H_2O ices are of fundamental importance in a broad range of scientific fields such as atmospheric chemistry,[1−3] cryobiology,[4] and astrochemistry.[5−11] There are several distinct H_2O ice phases. Among these, amorphous ice has gained considerable attention as a model system for studying amorphous and glassy materials, and phase transitions, and due to its importance in astrochemistry.[5−13]

Amorphous ice, also referred to as amorphous solid water (ASW), can be prepared by vapor depositing H_2O onto a cold substrate (<140 K).[14] It is a metastable phase of ice with respect to the crystalline phase.[15] It is believed to be the most abundant component of comets, interstellar clouds, and planetary rings.[5,16] ASW does not display properties of a single well-defined phase. For instance, there are discrepancies in the reported values of specific surface area,[17−19] glass transition temperature,[20,21] and the nature of supercooled water.[20] Recent studies show that ASW properties depend greatly on growth conditions[17] and the thermal history of the ASW.[18,22,23]

Several studies indicate that ASW can trap volatile gas molecules.[7,10,11,23−26] This implies that volatile species can be present in interstellar ices at temperatures higher than their sublimation temperature. The ability of ASW to trap molecules depends on its morphology.[24] Concentrations of trapped molecules also depend on how these molecules are deposited.[24,26] It was proposed that an increase in ASW temperature induces slight molecular rearrangements,[24] and these rearrangements close escape pathways for the trapped molecules.[24] Indeed, there is evidence of ASW reorganization at temperatures well below the ASW-to-cubic ice transition.[22]

Temperature-programmed desorption (TPD) and IR spectroscopic studies of thin ASW films (<100 layers) have shown that the release of trapped molecules occurs at several distinct temperatures.[7,9,23−28] This process does not depend on the binding energy of the guest molecules. The trapped molecules desorb during the phase transition, as well as during the sublimation of the cubic ice (CI) film. It is accepted that the release of guest molecules during the ASW-to-CI transition occurs through pathways present in ASW during the phase transition.[24]

The retention of guest molecules up to the CI sublimation temperature is not always observed.[7,9,11,24] It is unclear what mediates the ratio of trapped species released during the phase transition to trapped species that are retained within CI. Collings et al. reported that this ratio and the amount of guest species desorbing during CI sublimation depend on the ice film thickness.[26] It is not clear if this ratio can be manipulated (e.g., independent of ASW thickness) by changing deposition conditions. Additionally, the nature of the site from which these molecules desorb remains speculative. Ayotte et al.[24] have suggested that this could be due to molecules being trapped in a simple pore, trapped in a clathrate hydrate cage, or buried under the water overlayer. Several studies show that only a few molecules form clathrate hydrates under low-temperature and ultrahigh vacuum (UHV) conditions.[7,29]

In the present study, the above issues were examined by using a combination of Fourier transform infrared (FTIR) and TPD techniques. It was possible to monitor changes in the FTIR spectra of guest molecules trapped in the ASW, as well as the TPD traces of these trapped species. This permits comparison of FTIR and TPD spectra of the same samples, thereby providing information on the nature of the molecules that stay in ice after the phase transition. CO_2 has been shown to be a good candidate for probing ice morphology and studying the trapping and release of volatile molecules by ASW films.[23] Its large oscillator strength and narrow line widths facilitate the detection of small amounts of guest molecules and small frequency shifts.

2. Experimental Section

Experiments were carried out in a UHV chamber with a base pressure of $\sim 10^{-10}$ Torr. A schematic drawing of the arrange-

* Corresponding authors.

10.1021/jp074083i CCC: $37.00
Published on Web 11/30/2007

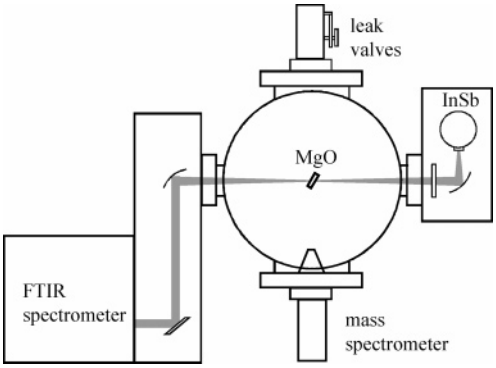

Figure 1. Schematic drawing of the experimental arrangement: IR radiation is reflected from a flat mirror and a focusing mirror (150 mm focal length) before entering the UHV chamber through a CaF_2 window. It passes through the rotatable MgO crystal and exits the chamber through a CaF_2 window. It passes through a wire grid polarizer and is focused (45 mm focal length) onto a 2 mm diameter InSb detector element. The path is purged to remove atmospheric water and carbon dioxide. Precision leak valves dose water and $^{13}CO_2$, and a residual gas analyzer with a narrow aperture observes molecules desorbed from the surface via TPD.

ment is given in Figure 1. The experimental strategy and arrangement have been described in detail elsewhere[23,30] and will be outlined briefly here. The chamber is equipped with instrumentation to perform transmission FTIR and TPD studies. TPD spectroscopy was performed using a residual gas analyzer (Stanford Research Systems, RGA 300). FTIR spectroscopy was carried out using a Nicolet Protegé 460 spectrometer with a liquid nitrogen cooled InSb detector. Infrared radiation entered and exited the chamber through CaF_2 windows. It was brought to a focus at the sample, and after exiting the chamber it was refocused onto the detector.

The substrate was a MgO single crystal (MTI) with typical dimensions of ~1 mm × 10 mm × 10 mm. This was obtained by cleaving a MgO crystal twice in a dry nitrogen atmosphere. A cleaved MgO crystal with fresh (100) surfaces was quickly inserted into the UHV chamber. After baking the chamber and reaching the base pressure, the substrate was annealed in oxygen to remove oxygen vacancies and contaminants from the MgO(100) surface.[30,31] The surface temperature was measured using a *k*-type thermocouple glued to the front edge of the crystal with a high-temperature ceramic adhesive (Aremco 569).

The surface holder, which was used in previous FTIR studies,[23] was modified to perform TPD (in addition to FTIR) and to keep the same level of sample cooling. Care was taken to minimize thermal gradients across the substrate. The substrate was attached to a thin copper plate (~0.3 mm × 10 mm × 14 mm) by laying the substrate on the plate and folding over two opposite edges of the plate onto the substrate. In this manner, only two thin strips (~1 mm × 10 mm) at the edges of the substrate were completely sandwiched by the plate. A square opening (~5 mm × 5 mm) in the middle of the copper plate allowed transmission FTIR experiments to be performed. The copper plate was connected with a stainless steel screw to one of two copper blocks attached to a liquid nitrogen reservoir. With the use of a sapphire disk and ceramic washers, these copper blocks were electrically isolated from each other and from the reservoir. The sample was resistively heated using a home-made heater cemented (Aremco 569) onto the back of the copper plate. The heater was made from a tantalum wire (~0.4 mm) that was isolated from the copper plate by a ceramic thermocouple insulator (Omega ORX-020132). The wire was bent several times to form a rectangular shape (~10 mm × 10 mm).

The reservoir was attached to a precision manipulator to provide *XYZ* translation and 360° rotation. A substrate temperature of ~90 K was obtained routinely by bubbling helium gas through liquid nitrogen in the reservoir. The sample temperature could be altered from 90 to 500 K and from room temperature to 700 K. The new surface holder design minimized mass spectrometer signals coming from the copper parts of the sample holder during TPD.

Purified and deionized H_2O was degassed by several freeze−pump−thaw cycles and dosed using a stainless steel tube (~4 mm diameter) connected to a leak valve. The distance from the tube to the substrate was ~50 mm. It was noticed that during backfilling of the chamber with H_2O (5×10^{-8} Torr) there was a small increase in the $m/e = 44$ (i.e., $^{12}CO_2^+$) signal. In addition, the mass spectrometer showed an increase of $m/e = 44$ signal during desorption of the H_2O film from the substrate, whereas the FTIR spectrum indicated clearly that there was no CO_2 present on the substrate. The source of the aforementioned CO_2 is unknown. To lessen such complications, $^{13}CO_2$ (Icon Isotopes, 99%) was used instead of $^{12}CO_2$. The $^{13}CO_2$ sample was introduced into the chamber through a separate leak valve and dosing line.

Substrates were heated to 400 K to desorb contaminants before performing experiments. FTIR spectra (200−500 scans) covering the region of 2000−4000 cm^{-1} were recorded at 1 cm^{-1} resolution. A background spectrum of the MgO(100) substrate was collected at 90 K. The substrate was tilted such that the angle between the propagation vector of the p-polarized IR radiation and the surface normal was 50°. In TPD experiments, a temperature ramp rate of ~1 K/s was used, and $m/e = 18$ (H_2O^+) and 45 ($^{13}CO_2^+$) were monitored with the mass spectrometer.

The thickness of a water film was estimated by comparing the integrated TPD intensity of the water film (approximately proportional to exposure time at constant dosing pressure) with that of a water monolayer. The water monolayer coverage was obtained using TPD, as in a previous study.[30] The $^{13}CO_2$ coverage could not be obtained easily from our experiments. The $^{13}CO_2$ TPD signal could not be calibrated due to the absence of a distinct $^{13}CO_2$ TPD feature that can be ascribed to the monolayer. This can be explained by a negligible difference in the binding energy of $^{13}CO_2$ molecules to $^{13}CO_2$ molecules and $^{13}CO_2$ molecules to the ASW interface or to the MgO(100) surface.[11,32,33]

3. Results

We have studied $^{13}CO_2$ interactions with amorphous and crystalline ice by means of TPD and FTIR spectroscopy. The experimental results consist mainly of TPD spectra of $^{13}CO_2$ desorbing from ASW and FTIR spectra of $^{13}CO_2$ (ν_3 region) trapped within the ASW film.

The $^{13}CO_2$ deposited on a MgO(100) surface at 90 K forms a polycrystalline film. The IR spectrum of the film exhibits two distinct bands (Figure 2a) that can be ascribed to the longitudinal (LO) and the transverse optical (TO) modes in crystalline $^{13}CO_2$.[34] Figure 2b shows the TPD spectrum of $^{13}CO_2$ desorbing from a MgO(100) surface. Only one feature, centered at 106 K, is evident. This peak corresponds to sublimation of $^{13}CO_2$. These results are similar to TPD results obtained from CO_2 on other surfaces.[26]

When $^{13}CO_2$ is deposited at high coverage on top of the ASW film at 90 K, three peaks are observed in the $^{13}CO_2$ TPD trace (Figure 3a). The TPD trace can be divided into two regions: low temperature (<110 K) and high temperature (>160 K).

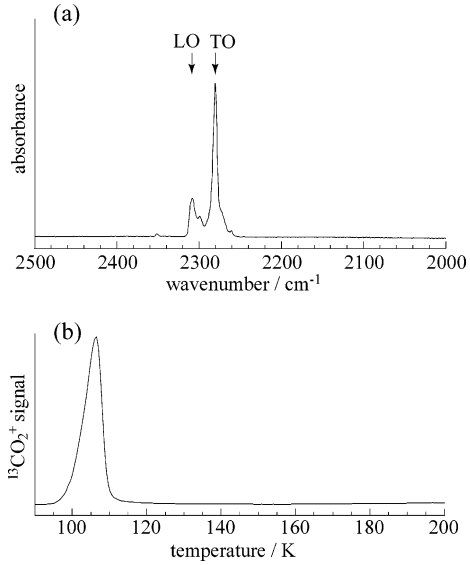

Figure 2. $^{13}CO_2$ was deposited (4×10^{-8} Torr, 3 min) onto MgO(100) at 90 K, at which time FTIR and TPD traces were recorded. Entries a and b show the $^{13}CO_2$ ν_3 spectral region and the TPD trace, respectively. The LO and TO modes of the $^{13}CO_2$ film are indicated in (a). TPD was carried out by heating the surface at 1 K/s while monitoring $m/e = 45$.

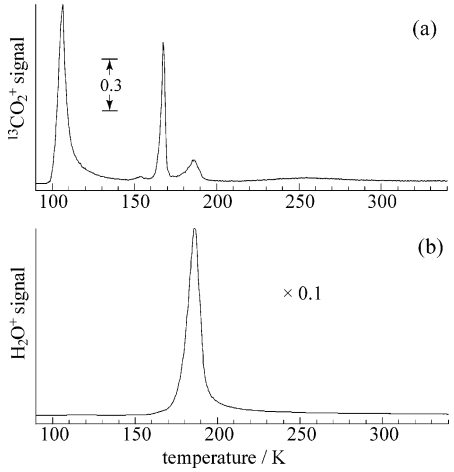

Figure 3. $^{13}CO_2$ was deposited (4×10^{-8} Torr, 30 s) onto an ASW film of ~40 layers (5×10^{-8} Torr, 8 min). H_2O and $^{13}CO_2$ desorption was monitored at $m/e = 18$ and 45, respectively. Parts a and b show TPD traces for CO_2 and H_2O, respectively. Note that the H_2O TPD trace is scaled by a factor of 0.1. The scale factor of 0.3 shown in (a) is for comparison with Figures 4−6.

The peak at 106 K is similar to the feature observed for CO_2 desorbing from MgO(100) and is thus attributed to $^{13}CO_2$ desorption from atop the ASW film. For ASW films of the same thickness, the intensity of this peak increases with $^{13}CO_2$ coverage.

The TPD features at 165 and 185 K are assigned to $^{13}CO_2$ desorbing from the interior of the ASW film. For ASW films of the same thickness with *low* $^{13}CO_2$ coverages, the $^{13}CO_2$ TPD traces display only two TPD features—at 165 and 185 K. The intensity of these peaks saturates as the $^{13}CO_2$ coverage increases and the 107 K feature appears. The intensity of the 107 K peak continues to increase as the $^{13}CO_2$ coverage increases. The small bump at 155 K is due to $^{13}CO_2$ desorption from the sample holder. This was determined from experiments in which the sample holder position was varied relative to the mass spectrometer aperture. The 165 K peak (also known as the volcano peak[35]) corresponds to $^{13}CO_2$ desorption from the ASW film

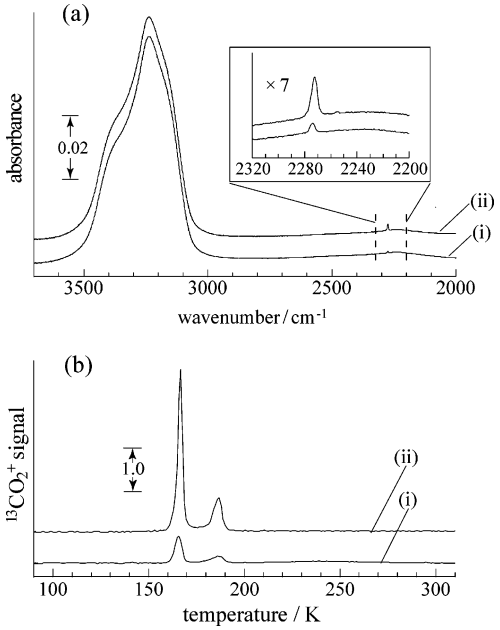

Figure 4. (a) FTIR spectra (p-polarization) of (i) $^{13}CO_2$ deposited atop ASW film (~40 layers) and (ii) $^{13}CO_2$ deposited before the ASW film (~40 layers). ASW formation and $^{13}CO_2$ deposition were carried out at 90 K. Each sample was annealed to 115 K and recooled to 90 K. CO_2 was deposited at 4×10^{-8} Torr for 30 s. The inset shows the expanded scale of the $^{13}CO_2$ ν_3 region. (b) TPD spectra of $^{13}CO_2$ recorded for the samples in (a): (i) ASW film (~40 layers) exposed to $^{13}CO_2$ and (ii) ASW film deposited onto $^{13}CO_2$ film (TPD spectra were recorded after FTIR spectra). The scale factor of 1.0 is for comparison with Figures 3, 5, and 6.

during the amorphous-to-cubic ice phase transition. The maximum peak intensity and the area of the 165 K peak are proportional to the ASW film thickness. The second peak (185 K) results from $^{13}CO_2$ that remains trapped after the ASW film has crystallized. The release of these $^{13}CO_2$ molecules occurs concurrently with desorption of the ice film (Figure 3b). Similar to the volcano peak, the maximum intensity and the area of this peak are proportional to the ASW film thickness.

FTIR spectra serve as good indicators of $^{13}CO_2$ in the ASW sample.[11,23] Figure 4a, trace i, shows the FTIR spectrum obtained after depositing $^{13}CO_2$ onto ASW at 90 K, annealing, and then recooling. Annealing the substrate to 115 K results in desorption of the solid $^{13}CO_2$ film atop ASW and the appearance of a residual band at 2275 cm^{-1}, similar to observations reported by Kumi et al.[23] Figure 4a, trace ii, depicts the FTIR spectrum obtained after depositing $^{13}CO_2$ *below* ASW at 90 K, annealing, and then recooling. Deposition of $^{13}CO_2$ before the formation of ASW leads to an increase in the 2275 cm^{-1} band intensity.

The $^{13}CO_2$ TPD traces (obtained after recording the FTIR spectra shown in Figure 4a) of $^{13}CO_2$ deposited atop ASW and $^{13}CO_2$ deposited before ASW formation (samples were annealed to 115 K) display the aforementioned two high-temperature TPD peaks. The intensities of both of these features are greater for the TPD trace from the sample in which $^{13}CO_2$ was deposited prior to ASW formation. However, the ratio of the peak area of the volcano peak to the peak area of the codesorption peak is the same for both samples, as seen in Figure 4b, i.e., this ratio does not depend on deposition sequence. In addition, it does not change with ice thickness.

Codeposition of $^{13}CO_2$ and H_2O increases the amount of $^{13}CO_2$ that desorbs during the phase transition. Figure 5b depicts $^{13}CO_2$ TPD traces obtained when $^{13}CO_2$ and H_2O are codeposited using separate dosers. For $^{13}CO_2$ partial pressures less than

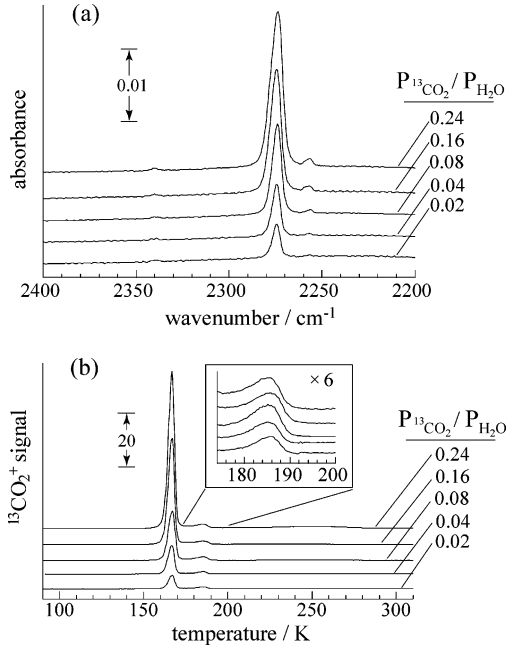

Figure 5. TPD and FTIR spectra of codeposited (through separate dosers) $^{13}CO_2$ with H_2O: H_2O pressures and exposure times were the same in all experiments (5×10^{-8} Torr, 8 min); $^{13}CO_2$ pressures are given as fractions of the H_2O pressure $P_{CO_2}/P_{H_2}O$. Samples were annealed to 115 K and recooled to 90 K before recording each trace. Spectra are offset for clarity. (a) FTIR spectra (p-polarization); the bumps at 2256 cm^{-1} are due to $^{13}C^{18}O^{16}O$. (b) TPD spectra; the inset shows an expanded scale of the $^{13}CO_2$ codesorption peak (i.e., $^{13}CO_2$ desorbing with the polycrystalline water film). TPD traces of H_2O were approximately the same.

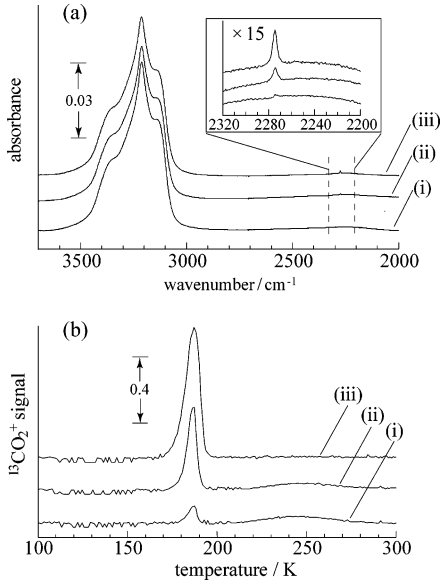

Figure 6. (a) FTIR spectra (p-polarization): (i) $^{13}CO_2$ deposited (4×10^{-8} Torr, 30 s) onto ASW film; (ii) $^{13}CO_2$ deposited (4×10^{-8} Torr, 30 s) before formation of ASW film; (iii) $^{13}CO_2$ (2×10^{-9} Torr) codeposited with H_2O. Each sample was annealed to 165 K and recooled to 90 K. The H_2O exposure was approximately the same (5×10^{-8} Torr, 8 min) for all experiments. The inset shows the expanded scale of the $^{13}CO_2$ ν_3 region. (b) TPD spectra were recorded for the samples in (a) immediately after recording the FTIR spectra.

0.25 of the H_2O partial pressure, there is no desorption in the low-temperature region. Only the two high-temperature (i.e., >160 K) features are present. The intensity of the volcano peak depends on the $^{13}CO_2$ partial pressure during deposition. The TPD codesorption feature at 185 K does not change significantly with $^{13}CO_2$ partial pressure.

The infrared absorption intensity of the ν_3 band depends on the partial pressure of $^{13}CO_2$ in the codeposition of $^{13}CO_2$ and H_2O (Figure 5a). The intensity of this band increases with $^{13}CO_2$ partial pressure. The area of the 2275 cm^{-1} band is approximately proportional to the amount of $^{13}CO_2$ that desorbs during thermal desorption, i.e., it is proportional to the areas of the volcano and codesorption peaks.

Annealing ASW to 165 K leads to crystallization. Most of the trapped $^{13}CO_2$ escapes during the ASW-to-CI transition. The intensity of the feature at 2275 cm^{-1} is reduced significantly after crystallization. Figure 6a shows FTIR spectra of three samples annealed to 165 K that were formed by depositing $^{13}CO_2$ atop ASW (trace i), depositing $^{13}CO_2$ underneath ASW (trace ii), and codepositing $^{13}CO_2$ and H_2O during ASW formation. The broad H_2O feature centered at 3250 cm^{-1} changes upon annealing to 165 K because of the ASW-to-CI phase transition.[36] For the samples used in Figure 6a, the 2275 cm^{-1} band has largest intensity for $^{13}CO_2$ codeposited with H_2O, and it is essentially zero for $^{13}CO_2$ deposited atop ASW.

The TPD trace of $^{13}CO_2$ trapped in cubic ice exhibits a single peak at 185 K. Figure 6b shows TPD traces of $^{13}CO_2$ desorbing from samples annealed to 165 K, which were formed by depositing $^{13}CO_2$ atop ASW (trace i), depositing $^{13}CO_2$ underneath ASW (trace ii), and codepositing $^{13}CO_2$ and H_2O during ASW formation. The intensities of the 185 K TPD peaks behave similarly to the $^{13}CO_2$ IR feature. Namely, the maximum peak intensity and the peak area of the $^{13}CO_2$ TPD peak at 185 K are proportional to the maximum band intensity and integrated band area of the $^{13}CO_2$ 2275 cm^{-1} IR feature, respectively.

4. Discussion

The inclusion of guest molecules into ASW films depends on how these molecules are deposited and on film structure.[17,24,26] It is widely accepted that some of the guest molecules within porous ASW films can be trapped upon annealing.[7,9−11,25,26,37,38] The transport and trapping of guest molecules depend on the ASW pore network, the trapping sites, and changes that occur in the network upon annealing. The nature of trapping sites is hard to deduce by using TPD alone.[24] The present study of $^{13}CO_2$ transport and trapping in ASW films combines TPD and FTIR. Due to its sensitivity to the local environment and changes that occur upon annealing, the IR signature of the trapped molecules provides useful information.

It has been shown that CO_2 guest molecules dosed at 90 K possess enough mobility to diffuse into the porous ASW films.[23] Upon saturation of the sites within the film that can be accessed (i.e., from either above or below), CO_2 forms a solid crystalline film atop ASW.[23] The TPD peak at 107 K is due to $^{13}CO_2$ desorbing from the ASW surface and from sites within the film that remain connected to the surface even after annealing (Figure 3). The TPD spectrum of $^{13}CO_2$ deposited underneath the film also shows the 107 K peak. This low-temperature peak shifts to slightly higher temperatures with increasing film thickness. The presence of the 107 K peak suggests that the ASW overlayer is porous enough to provide pathways connected to the ASW surface for $^{13}CO_2$ molecules to escape. Other studies showed that for dense ASW films guest molecules deposited underneath ASW stay trapped until the ice phase transition.[24]

When $^{13}CO_2$ is deposited on top or underneath the ASW film, there is no appreciable desorption of $^{13}CO_2$ in the temperature range of 115−160 K. Molecules trapped during thermally induced changes in ASW morphology do not escape until 160 K. The FTIR spectra (Figures 4a and 5a) show the presence

of trapped $^{13}CO_2$ within the film. The amount of trapped $^{13}CO_2$ depends strongly on whether $^{13}CO_2$ was deposited on top or underneath the ASW.

The ASW film is able to trap ~4 times more molecules when $^{13}CO_2$ is deposited underneath it. This number was obtained by comparing the areas of the $^{13}CO_2$ ν_3 bands for $^{13}CO_2$ deposited atop and under the ASW (Figure 4a). A similar result was obtained by comparing the amount of trapped $^{13}CO_2$ desorbing during TPD (which is proportional to the area of the high-temperature TPD peaks) for $^{13}CO_2$ deposited atop and under the ASW (Figure 4b). This suggests that guest molecules deposited underneath the porous ASW film sample more binding sites in the ASW as the temperature rises during annealing. This is intuitive, because they are inhibited from evaporating relative to those that access the bulk from above.

Most of the trapped $^{13}CO_2$ escapes during the ASW-to-CI phase transition, and the rest desorbs during cubic ice removal at 185 K. The abrupt release of guest molecules during crystallization apparently occurs through connected desorption pathways in the film; these pathways can be formed during the phase transition.[24,35] However, some molecules are not released from the cubic ice until the sublimation of the film (Figure 3). It is unlikely that these molecules simply reside under the H_2O overlayer, because when ASW is deposited on top of $^{13}CO_2$ the amount of trapped $^{13}CO_2$ is proportional to the ice film thickness. Probably these molecules reside within the cubic ice film. Presumably, they cannot escape from sites within the film because no connection to the outer surface has been formed during crystallization.

The TPD experiments show that the ratio of the areas of the codesorption peak to the volcano peak does not change for $^{13}CO_2$ deposited atop or underneath the ASW. This conclusion can also be made by comparing the areas of the $^{13}CO_2$ ν_3 band for $^{13}CO_2$ isolated after annealing to 115 and 165 K. This supports the previous statement that depositing $^{13}CO_2$ molecules underneath the ASW simply allows them to better sample sites in the ASW film during transport through it.

Codeposition of $^{13}CO_2$ and H_2O affects trapping and desorption. For $P_{CO_2}/P_{H_2O} < 0.25$, all of the $^{13}CO_2$ that is absorbed by ASW becomes trapped upon annealing. The amount of trapped $^{13}CO_2$ is proportional to its partial pressure. The majority of these molecules are released during crystallization. In fact, both TPD and IR reveal that different $^{13}CO_2$ partial pressures (within 0.02−0.25 of the H_2O partial pressure) do not affect significantly the amount of $^{13}CO_2$ released during removal of the cubic ice film at 185 K. However, the amount of $^{13}CO_2$ that desorbs when $^{13}CO_2$ is codeposited with H_2O is larger than the amount that desorbs when $^{13}CO_2$ is deposited atop or under the ASW film.

Codeposition at $P_{CO_2}/P_{H_2O} > 0.25$ leads to saturation of the high-temperature TPD features. It also leads to appearance of the low-temperature TPD peak at 107 K, broadening of the $^{13}CO_2$ ν_3 feature, and eventually (with increasing $^{13}CO_2$ partial pressures), appearance of the LO and TO bands. All of these confirm the formation of solid polycrystalline $^{13}CO_2$ atop the ASW. Thus, there is saturation of the trapping sites within the ASW film at high $^{13}CO_2$ pressures. The hydrogen-bonding interaction between H_2O molecules is much stronger than H_2O-CO_2 and CO_2-CO_2 interactions.[11,39] Based on the saturation of the trapping sites and the aforementioned interaction strength, we speculate that codeposition of $^{13}CO_2$ does not alter the ASW structure significantly, under the present experimental conditions. Codeposition probably affects how the $^{13}CO_2$ molecules sample sites within the ASW film (i.e., codeposition allows $^{13}CO_2$ to populate sites that are not directly connected to the vacuum).

The largest amount of $^{13}CO_2$ that can be trapped during codeposition is roughly 1 $^{13}CO_2$ molecule for every 30 H_2O molecules. This ratio was obtained by comparing the area of the H_2O TPD peak to the area of the high-temperature $^{13}CO_2$ TPD peaks. Approximately the same ratio is obtained using the integrated adsorption cross section per molecule of the CO_2 ν_3 band,[40] together with the assumption that the ASW layer thickness is 0.4 nm and the ASW density is 0.9 g cm^{-3}. Most likely this ratio will depend on the deposition conditions, e.g., via a collimated molecular beam or when much thicker ASW films are created.[7,17,41]

Species that desorb during the sublimation of the ice film can be isolated in the film by annealing ASW−CO_2 samples to 165 K. The position of the $^{13}CO_2$ ν_3 band at 2275 cm^{-1} is the same for samples annealed to 115 and 165 K (compare Figures 4a, 5a, and 6a). The robustness of the $^{13}CO_2$ ν_3 band frequency suggests that trapping sites for the $^{13}CO_2$ that escapes from the ice during the phase transition are similar to those that desorb during ice film depletion. Previous IR studies of CO_2 clathrate hydrates[42−44] reported CO_2 ν_3 band positions that are shifted from the ν_3 band position for CO_2 trapped in ASW. Thus, it is unlikely that the release of $^{13}CO_2$ at 185 K (concurrent with sublimation of ice film) is due to molecules trapped in clathrate hydrate cages. We speculate that this release is related to molecules trapped in cavities within the ASW film similar to ones that trap the $^{13}CO_2$ released during the crystallization.

The area of the $^{13}CO_2$ ν_3 band is proportional to the number of trapped $^{13}CO_2$ molecules and the infrared absorption cross section of the $^{13}CO_2$ molecule. The area of the $^{13}CO_2$ TPD peaks at 165 and 185 K is proportional to the number of desorbing $^{13}CO_2$ molecules. Thus, the ratio of the $^{13}CO_2$ ν_3 band area to the total area of the $^{13}CO_2$ TPD peaks at 165 and 185 K (or only the area of the 185 K peak if the sample was annealed to 165 K) should be proportional to the IR integrated cross section per molecule. In our experiments, this ratio was the same (within a 25% error margin) for $^{13}CO_2$ trapped within ASW ($^{13}CO_2$ deposited atop ASW, under ASW, and codeposited with H_2O) and for $^{13}CO_2$ solid films. This indicates little change in the $^{13}CO_2$ infrared transition dipole moments in our experiments. This suggests that there is no significant difference in the local environment for $^{13}CO_2$ molecules trapped in the various sites.

The general assumption that ASW films are always porous is not always true. For instance, several studies show that the porosity and density of amorphous ice films significantly depend on factors such as the growth temperature and angle of deposition.[6,17,41] Only porous ASW is believed to trap guest molecules residing within its pores by subtle alterations in its structure. Moreover, for guest species to be retained, they must be located within pores during these structural alterations. At a specified temperature, the residence times of a molecule in an ASW pore depend on the molecule as well as its desorption rate. Thus, experimental conditions conducive to trapping different species in porous ASW are expected to vary. Our observations suggest that (i) the ASW films we prepare at 90 K are porous and (ii) at 105 K, some $^{13}CO_2$ is unable to desorb prior to the aforementioned ASW structural changes.

We were also able to alter the number of $^{13}CO_2$ guest molecules in the film by varying the method of deposition (i.e., on top of the ASW, underneath the ASW, and codeposition). It has been suggested that the codeposition of H_2O with guest species may influence the structure of the ASW film.[11,26] No significant differences in the desorption temperatures and

the IR signatures of the trapped species were discernible for the various methods of guest molecule deposition used in the studies reported herein. However, as mentioned previously, the ratio of trapped molecules released during the phase transition to trapped molecules that codesorb with crystalline ice depends upon the method of deposition.

Bar-Nun and co-workers observed that molecules trapped in thick (several micrometers) ASW films following codeposition were ejected at several distinct temperatures.[7,38] In contrast, our results indicate that the release of trapped species occurs in two distinct temperature regimes, which is consistent with other studies of thin (less than 1 μm) ASW films. It is possible therefore that there may be slight differences in the processes mediating the release of trapped species in thick and thin ASW films.

Acknowledgment. This research has been supported by grants from the Air Force Office of Scientific Research (F49620-01-1-0071) and the Army Research Office (W911NF-07-1-0081). The authors benefited from discussions with Oscar Rebolledo-Mayoral.

References and Notes

(1) Berland, B. S.; Brown, D. E.; Tolbert, M. A.; George, S. M. *Geophys. Res. Lett.* **1995**, *22*, 3493.
(2) Graham, J. D.; Roberts, J. T. *J. Phys. Chem.* **1994**, *98*, 5974.
(3) Solomon, S. *Nature* **1990**, *347*, 347.
(4) Rasmussen, D. H.; MacKenzie, A. P. *J. Phys. Chem.* **1971**, *75*, 967.
(5) Jenniskens, P.; Blake, D. F. *Science* **1994**, *265*, 753.
(6) Stevenson, K. P.; Kimmel, G. A.; Dohnalek, Z.; Smith, R. S.; Kay, B. D. *Science* **1999**, *283*, 1505.
(7) Bar-Nun, A.; Herman, G.; Laufer, D.; Rappaport, M. L. *Icarus* **1985**, *63*, 317.
(8) Allamandola, L. J.; Sandford, S. A.; Tielens, A. G. G. M.; Herbst, T. M. *Astrophys. J.* **1992**, *399*, 134.
(9) Allamandola, L. J.; Sandford, S. A.; Valero, G. J. *Icarus* **1988**, *76*, 225.
(10) Sandford, S. A.; Allamandola, L. J. *Icarus* **1988**, *76*, 201.
(11) Sandford, S. A.; Allamandola, L. J. *Astrophys. J.* **1990**, *355*, 357.
(12) Angell, C. A. *Science* **1995**, *267*, 1924.
(13) Kouchi, A.; Kuroda, T. *Nature* **1990**, *344*, 134.
(14) Sceats, M. G.; Rice, S. A. In *Water: A Comprehensive Treatise*; Franks, F., Ed.; Plenum Press: New York, 1982; Vol. 7, p 83.
(15) Angell, C. A. *Annu. Rev. Phys. Chem.* **1983**, *34*, 593.
(16) Smoluchowski, R. *Science* **1978**, *201*, 809.
(17) Kimmel, G. A.; Stevenson, K. P.; Dohnalek, Z.; Smith, R. S.; Kay, B. D. *J. Chem. Phys.* **2001**, *114*, 5284.
(18) Manca, C.; Martin, C.; Roubin, P. *Chem. Phys. Lett.* **2002**, *364*, 220.
(19) Pletzer, R.; Mayer, E. *J. Chem. Phys.* **1989**, *90*, 5207.
(20) McClure, S. M.; Safarik, D. J.; Truskett, T. M.; Mullins, C. B. *J. Phys. Chem. B* **2006**, *110*, 11033.
(21) Smith, R. S.; Kay, B. D. *Nature* **1999**, *398*, 788.
(22) Manca, C.; Martin, C.; Roubin, P. *Chem. Phys.* **2004**, *300*, 53.
(23) Kumi, G.; Malyk, S.; Hawkins, S.; Reisler, H.; Wittig, C. *J. Phys. Chem. A* **2006**, *110*, 2097.
(24) Ayotte, P.; Smith, R. S.; Stevenson, K. P.; Dohnalek, Z.; Kimmel, G. A.; Kay, B. D. *J. Geophys. Res., [Planets]* **2001**, *106*, 33387.
(25) Hudson, R. L.; Donn, B. *Icarus* **1991**, *94*, 326.
(26) Collings, M. P.; Anderson, M. A.; Chen, R.; Dever, J. W.; Viti, S.; Williams, D. A.; McCoustra, M. R. S. *Mon. Not. R. Astron. Soc.* **2004**, *354*, 1133.
(27) Graham, J. D.; Roberts, J. T.; Brown, L. A.; Vaida, V. *J. Phys. Chem.* **1996**, *100*, 3115.
(28) Schaff, J. E.; Roberts, J. T. *Langmuir* **1998**, *14*, 1478.
(29) Notesco, G.; Bar-Nun, A. *Icarus* **2000**, *148*, 456.
(30) Hawkins, S.; Kumi, G.; Malyk, S.; Reisler, H.; Wittig, C. *Chem. Phys. Lett.* **2005**, *404*, 19.
(31) Korolik, M.; Suchan, M. M.; Johnson, M. J.; Arnold, D. W.; Reisler, H.; Wittig, C. *Chem. Phys. Lett.* **2000**, *326*, 11.
(32) Briquez, S.; Lakhlifi, A.; Picaud, S.; Girardet, C. *Chem. Phys.* **1995**, *194*, 65.
(33) Andersson, P. U.; Nagard, M. B.; Witt, G.; Pettersson, J. B. C. *J. Phys. Chem. A* **2004**, *108*, 4627.
(34) Ovchinnikov, M. A.; Wight, C. A. *J. Chem. Phys.* **1993**, *99*, 3374.
(35) Smith, R. S.; Huang, C.; Wong, E. K. L.; Kay, B. D. *Phys. Rev. Lett.* **1997**, *79*, 909.
(36) Hagen, W.; Tielens, A. G. G. M.; Greenberg, J. M. *Chem. Phys.* **1981**, *56*, 367.
(37) Bar-Nun, A.; Dror, J.; Kochavi, E.; Laufer, D. *Phys. Rev. B* **1987**, *35*, 2427.
(38) Bar-Nun, A.; Kleinfeld, I.; Kochavi, E. *Phys. Rev. B* **1988**, *38*, 7749.
(39) Smith, R. S.; Kay, B. D. *Surf. Rev. Lett.* **1997**, *4*, 781.
(40) Yamada, H.; Person, W. B. *J. Chem. Phys.* **1964**, *41*, 2478.
(41) Dohnalek, Z.; Kimmel, G. A.; Ayotte, P.; Smith, R. S.; Kay, B. D. *J. Chem. Phys.* **2003**, *118*, 364.
(42) Blake, D.; Allamandola, L.; Sandford, S.; Hudgins, D.; Freund, F. *Science* **1991**, *254*, 548.
(43) Fleyfel, F.; Devlin, J. P. *J. Phys. Chem.* **1991**, *95*, 3811.
(44) Hernandez, J.; Uras, N.; Devlin, J. P. *J. Phys. Chem. B* **1998**, *102*, 4526.